Extending the high-order-harmonic spectrum using surface plasmon polaritons

H. Ebadian and M. Mohebbi*

Department of Physics, Faculty of Science, Vali-e-Asr University of Rafsanjan, P.O. Box 77139-36417, Rafsanjan, Iran

(Received 20 January 2017; published 21 August 2017)

Nanoparticle assisted high-order-harmonic generation by low-intensity ultrashort laser pulses in hydrogen atomic gas is studied. This work is based on surface plasmon-polariton coupling in metal-insulator-metal structures. The necessary laser intensity is provided by enhancement of the incident laser power in the vicinity of bowtie nanoparticles installed on an insulator-metal structure. The inhomogeneous electric field distribution in the Au nanobowtie gap region is investigated. Simulations show that the insulator layer installed on the Au metal film that supports the plasmon-polariton interactions has a dramatic effect on the field enhancement factor. High-order-harmonic generation cutoffs for different arrangements are calculated and results show that the metal-insulator-metal structure is an excellent device for high-order-harmonic generation purposes. Also, the harmonic cutoff order is extended to more than 170, which is a considerable value and will be an efficient source for extreme ultraviolet radiation.

DOI: 10.1103/PhysRevA.96.023415

I. INTRODUCTION

Today, nonlinear optical phenomena are powerful apparatuses for scientific investigations. After the invention of lasers nonlinear optics developed more rapidly. In addition, ultrafast Ti:sapphire lasers with very high optical intensities (more than 10^{13} W/cm^2) opened a new horizon for advancement of nonlinear processes. High-order-harmonic generation (HHG) experiments have been produced in a gas medium, and the laser intensity should be more than 10^{14} W/cm^2 to initiate the HHG process. From a laser designer's point of view, such a high-power laser can be produced only from a complexly designed multiamplifier laser system. The ultrashort output of a Ti:sapphire laser oscillator should be, first, stretched to nanosecond pulses, then amplified in multiple amplifier stages, and, finally, compressed again to ultrashort pulses—and this is a tedious and expensive process. However, the elimination of complex and expensive amplifiers and the opportunity to perform HHG at megahertz repetition rates can significantly extend the capability for extreme vacuum ultraviolet generation and attosecond pump-probe spectroscopy [1]. An interesting experiment has been reported based on HHG near metal nanostructures. Nanojoule pulses directly from a laser oscillator have demonstrated HHG by exploiting the local field enhancement (FE) near a metallic bowtie-shaped gold nanoelement [2]. In that work, gold bowtie nanostructures were used in the argon gas medium. Moreover, research on extreme ultraviolet (EUV) attosecond pulses via HHG at megahertz repetition rates is in progress [3,4]. The incident electromagnetic field could be enhanced to several orders of magnitude, if one could design a nanoantenna that produces "hot spots." The plasmonic resonances observed in such structures open the possibility of building antennas operating in the visible spectrum. So far, in many papers, field enhancement in nanodimers has been theoretically and experimentally investigated [5–8]. Geometrical parameters such as antenna length, gap size, and angles can influence the antenna FE factor and spectral response. For example, in [5], the optical properties of different types of antennas have been discussed. Husakou *et al.* [1] explained the mechanism behind HHG based on plasmonics. They presented a semiclassical model for plasmon-enhanced high-order-harmonic generation near metal nanostructures and showed that, besides the FE, both the inhomogeneity of the enhanced local fields and electron absorption by the metal surface play an important role in the HHG process and lead to the generation of even harmonics and a significantly increased cutoff. In addition, they used silver-coated nanocones and bowtie antennas in the simulation. In [9], Park and coworkers demonstrated a three-dimensional (3D) metallic waveguide for the plasmonic generation of ultrashort EUV pulses by means of field enhancement using surface plasmon polaritons (SPPs). The intensity enhancement factor was about 350, which allowed generation up to the 43rd harmonic in xenon gas with the modest incident intensity of 10^{13} W/cm^2. Ciappina *et al.* investigated HHG resulting from the illumination of plasmonic nanostructures with a short laser pulse of long wavelength [10]. Shaaran *et al.* theoretically demonstrated that the strong inhomogeneity of this laser field plays an important role in the HHG process, leading to a significant increase in the harmonic-cutoff energy [11]. The electron dynamics in the vicinity of bowtie-shaped metallic nanostructures and the effect of the gas population on harmonic emission is investigated in [12,13]. In addition, the HHG spectrum of hydrogen atoms near dimers with different shapes is investigated [14]. In this work we would like to present a new type of HHG device. To the best of our knowledge, there is no work on high-order-harmonic generation in plasmon-polariton devices. Efforts are made to locate the resonance wavelength of the enhanced plasmonic field in the spectrum output of a Ti:sapphire laser using the optimization process. In our simulation, the output beam emitted from a modest femtosecond oscillator is directly focused onto the nanostructure with a pulse intensity of only 10^{11} W/cm^2 (below the damage threshold). The FE factor exceeds 30 dB, which is sufficient to produce soft x-ray emission, injection with a hydrogen gas jet. Here, we present a detailed analysis of high-order-harmonic generation in a plasmon-polariton structure. The effect of a nonmetal substrate and metal thin film on the FE factor is investigated.

*M.Mohebbi@vru.ac.ir

The interaction between SPPs and localized surface plasmons (LSPs) in a nanostructure and the resultant HHG spectrum in hydrogen atomic gas are evaluated. We organize this paper as follows: First, we take a glance at SPP and LSP physics and plasmonic nanoantennas. Then we investigate the electromagnetic coupling between a metal nanoparticle array and a metallic surface. Next, the simulation results of electric field enhancement factors of metal-insulator-metal (MIM) structures by 3D finite-difference time domain are presented, and, finally, the HHG spectrum of different structures is analyzed. In order to utilize the higher harmonic generation, we combine the numerical solution of the time-dependent Schrödinger equation (TDSE) with the electric fields obtained from plasmonic nanostructure simulations. Then the influence of the different parameters (shape, spacer thickness, and array effect) on the field enhancement and spectral response is discussed. We employ a classical analysis to extract more detailed information from the TDSE results and the extended harmonic spectra. Unless otherwise stated, atomic units are used throughout this paper.

II. PLASMONIC NANOANTENNAS

A plasmon is a quantum of plasma oscillation of the free electrons, and the free electron gas has a collective oscillation relative to the fixed positive ions in a metal. Plasmons with collective oscillation of the free electrons exhibit unique optical properties. Surface plasmons are those plasmons with collective electron oscillations that are confined to an interface between a metal and a dielectric. Furthermore, the combined excitation is called a surface plasmon polariton when a surface plasmon is coupled with a photon. SPPs are surface electromagnetic waves that propagate along the interface between the metal and the dielectric. The main difference between SPPs and LSPs is that SPPs are propagating surface waves, while LSPs are nonpropagating excitations of the free electrons of metallic structures coupled to the electromagnetic field. Furthermore, the curved surface of the bounded geometries (e.g., nanoparticles) demonstrates an effective restoring force on the driven electrons, resulting in resonance occurring on the surface, called surface plasmon resonance or localized surface plasmon resonance (e.g., for metallic nanostructures). On the other hand, the excitation conditions are different for LSPs and SPPs. LSPs (LSPR) can be excited by direct light illumination, whereas SPPs can be excited by matching the frequency and the momentum between the excitation light and the SPPs. The most common approach to excitation of surface plasmons is by means of a prism coupler and the attenuated total reflection method, known as kretschmann geometry and Otto geometry. Another approach to optical excitation of surface plasmons is based on the diffraction of light on a diffraction grating. In this method, a light wave is incident from a dielectric medium on a metal grating. Based on the short penetration depths of the electric fields of SPPs in the dielectric and the metal, the electric fields of SPPs are concentrated mainly near the interface, and the field concentration is remarkably enhanced at the interface. Nevertheless, the field concentration of SPPs diminishes rapidly away from the interface along the propagation direction, and the field concentration is higher in the dielectric than in the metal. The excited SPP waves have associated evanescent fields that penetrate into both the dielectric and the metal; they are spatially decaying fields in a direction normal to the interface [15].

III. ELECTROMAGNETIC COUPLING BETWEEN A METAL NANOPARTICLE AND A METALLIC SURFACE

So far, various plasmonic structures with a large intensity enhancement factor have been demonstrated theoretically and experimentally. Also, the electromagnetic coupling between 2D gratings and metal nanoparticles is investigated. The coupling between a metallic nanoparticle and a metallic thin film separated by a dielectric spacer, known as a metal-insulator-metal structure, was studied intensely for nanoantenna applications [16–18]. The coupling between an array made of gold nanoparticles and a gold metallic film was investigated in [17]. The MIM cavity confines light in the form of SPPs along the surface of the metallic film and leads to Fabry-Perot resonances along the direction perpendicular to the film [19,20]. Those studies also reported multipeaks in the extinction spectra attributed to resonant modes of the hybrid system, resulting from the coupling between the localized plasmon of the nanoparticles and the underlying surface plasmon mode. In [21] the coupling effect between grating diffraction and localized surface plasmons in 2D gold nanoparticle arrays in water was investigated and the authors concluded that it leads to narrow near-infrared resonance peaks in measured far-field extinction spectra. Then, more precisely, Crozier *et al.* investigated the interaction between localized and propagating surface plasmons in a structure consisting of a 2D periodic gold nanoparticle array, a SiO_2 spacer, and a gold film. Gold disks with periods varying from 620 to 880 nm diameters varying from 100 to 170 nm, and a 40-nm thickness were used. Anticrossing behavior of the resonance positions in the reflection spectra indicated a strong coupling between the LSP on the gold nanoparticles and the propagating surface plasmon on the gold film. The enhancement factor for a 2D nanodisk array on a gold film was about 10^4 [22].

The coupling strength between LSPR and SPPs will be affected by the size, shape, and arrangement period of nanoparticles and the thickness of the metal. Therefore different electric FE factors will be observed. Montgomery *et al.* proposed a plasmonic structure with a gold nanosphere array on a silver film, whose EF reaches 10^4. Hatab *et al.* realized an enhancement factor exceeding 10^5 in a free-standing gold nanobowtie array [23].

In these works, only one kind of nanoparticle is taken into account when constructing the arrays. A new structure, called a hybrid nanoparticle array, was proposed by Zhou *et al.* In this plasmonic scheme, the nanostructure is made of two kinds of nanoparticles and the enhancement factor is about 10^6 [24].

Usually plasmonic nanoantennas use different coupling mechanisms. A nanoantenna can be an isolated system in vacuum, or can be installed on an insulator-metal structure, or can be part of a regular array. Lin *et al.* considered all three types of coupling mechanisms together and proposed exploiting the coordinated multiple coupling in plasmonic nanoantennas to optimize the spectral tunability and the local field enhancement [25]. As a result, a huge electric field enhancement will be achieved. Comparing these enhancement

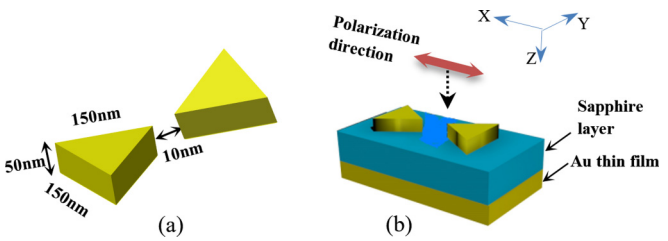

FIG. 1. (a) Sketch of the bowtie nanostructure. (b) MIM arrangement and incident polarized field.

factors, we concluded that because of its huge enhancement factors, the MIM structure will be an excellent device for extending the cutoffs of higher-order harmonics in rare gases or hydrogen atomic gas. This setup will have a good capability for soft x-ray generation, spectroscopy, and attosecond investigations.

IV. SIMULATIONS OF FIELD ENHANCEMENT

In previous studies, it has been shown that nanobowties can excite the SPP mode along a metal film efficiently. The electric FE of a nanobowtie can realize a large intensity enhancement factor due to its sharp corners and small gap [5,7,26,27]. Therefore, in the MIM structure, we adopt both a nanobowtie and a metal film as a unit plasmonic device and expect a larger local intensity enhancement factor.

It is well known that the surface charge density at a sharp corner can be extremely high because of the stronger localization of the electromagnetic field. In contrast, the electromagnetic field is less able to localize at the rounded corners because of the coarse surface charge density at those corners. Therefore, the electric field enhancement decreased when the curvature radius was increased. By varying the fabrication method, for example, by increasing the dosage of the electron beam, the tip curvature was controlled. The effect of the finite tip curvature of metal bowties (prisms) on the electric field enhancement factors and extinction efficiency has been investigated in detail [27–30]. Surely, in the fabrication process, it is hard to produce prisms with identical tip curvatures, because it is a random process. As an example, the effect of tip curvature on plasmonic properties for a round and a sharp prism dimer is investigated [27]. A sharp prism (8-nm radius of curvature) shows a field enhancement factor of about 380×, while a rounded prism (28-nm radius of curvature) shows an FE factor of about 190× (see also [29]). In this work, our emphasis is on the MIM structure, which induces more field enhancement factors than in the experiments by Kim *et al.* [2]. This advantage is due to the plasmon polariton effect. To use a procedure similar to that in the work of Kim *et al.*, to eliminate tip curvature selection, and for simplicity, we assumed bowties with sharp tips. In Sec. V, we see that the cutoff frequencies in our scheme (with sharp tips) are much higher than in the results of Kim *et al.* (without metal layer and with sharp tips). We think that, practically and under the same conditions, our scheme will be more efficient than HHG devices with no metal layer.

The plasmonic structure and the MIM arrangement are shown in Figs. 1(a) and 1(b). The nanobowtie is made of two similar triangles with an equilateral length of 150 nm, a thickness $t = 50$ nm, and a gap between tips of 10 nm. In our numerical modeling, the source is assumed to be an ultrashort femtosecond pulse from a Ti:sapphire laser with an intensity of 10^{11} W/cm^2 that is polarized in the x direction and propagates along the z direction. The incident electric field is $E(t) = E_0 f(t)(\cos(\omega_0 t))$, where E_0 is the laser field amplitude, $f(t) = \cos^2(\frac{\pi t}{\tau})$ is the laser field envelope, and $\omega = 0.057$ and $\tau = 5$ fs are the corresponding frequency and duration. In this paper we use the finite-difference time domain method to simulate FE factors for all nanostructures [31,32].

A. Effect of the insulator on the field enhancement factor for a single bowtie

The substrate is an essential part of any photonic or optoelectronic nanostructured device not only due to its own contribution to the optical response, but also due to the specific interactions with the supported nanostructure. We know that stronger field confinement can be obtained for sharper geometries such as triangular nanostructures. In practical applications, and also in our work, metallic nanoparticles contact the substrate directly. The field intensities in the top region and the bottom region of the nanostructures will be

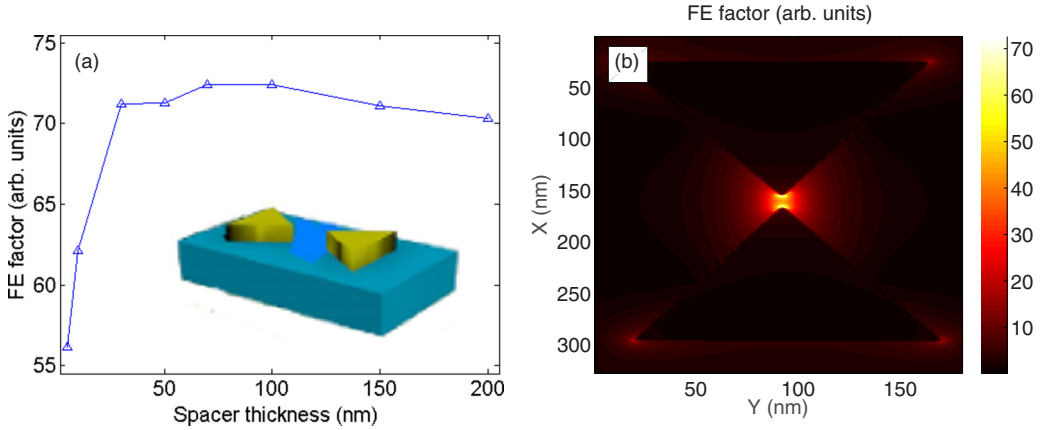

FIG. 2. (a) FE factor vs sapphire spacer thickness. (b) Corresponding magnitude of electric field distributions in the xy plane for a 70-nm sapphire spacer.

different. The bottom region of the metallic nanostructure is in contact with the insulator sapphire layer, while the top region is in contact with air, thus the bottom region has a locally higher effective refractive index. A light wave tends to localize itself mostly in a medium with a higher refractive index [33]. The simulation results are in agreement with this, showing a stronger field intensity in the bottom region than in the top region. In this section we study the nanobowtie in two positions: in vacuum and on a sapphire substrate. In both cases the x-direction polarized light is propagated in the z direction. The FE factor is measured 10 nm above the insulator layer. First we consider the bowtie nanoantenna of Fig. 1(a) in vacuum without any spacer or metal film. The results show an FE factor of approximately 45×. Next we placed the above nanoantenna on a sapphire layer (as shown in the inset in Fig. 2(a)). Because of the importance of the sapphire thickness to the FE factor, we study different insulator layers—5, 10, 30, 50, 70, 100, 150, and 200 nm—and the maximum FE factors are plotted in Fig. 2(a). The maximum FE factor for a nanoantenna installed on a 70-nm sapphire layer is about 70, which is more than the vacuum value (45). The corresponding magnitude of electric field distributions in the xy plane is shown in Fig. 2(b). The horizontal and vertical axes show the simulation region dimensions and the maximum FE is in the gap between the tips of the nanobowties.

B. Study of MIM structure for a single bowtie

In this section the metal-insulator-metal structure is considered. As shown in Fig. 2(a), the 70-nm sapphire layer has the maximum FE factor, hence we installed the gold nanobowtie on a 70-nm sapphire layer and attached them to a 20-nm gold thin film [Fig. 1(b)]. The structure is illuminated by x-directed polarized light propagating in the z direction. The maximum FE factor is about 100. The corresponding magnitude of electric field distributions in the xy plane is shown in Fig. 3. In comparison with Fig. 2(b), we deduce that the MIM structure has a better FE factor than a nanoantenna on a s layer, which is due to the surface plasmon–polariton coupling effect.

Usually the HHG process is derived with an ultrafast tunable Ti:sapphire laser in the range of 700–900 nm and

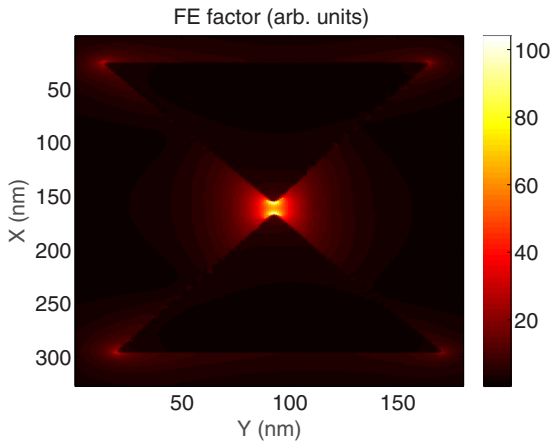

FIG. 3. Magnitude of electric field distributions in the xy plane for a MIM with a 70-nm sapphire layer.

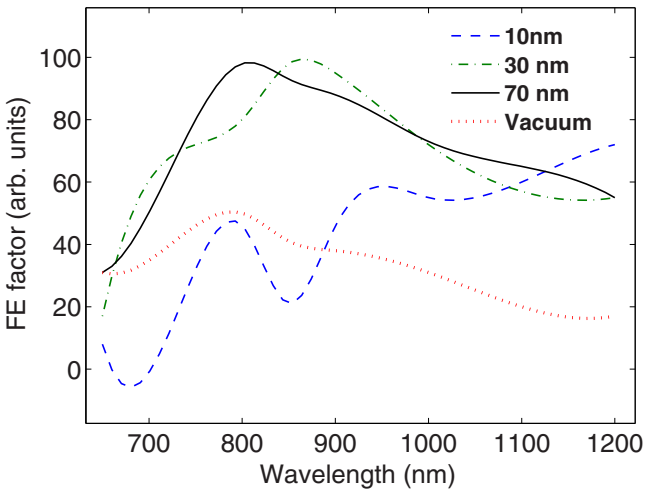

FIG. 4. Spectral responses of the single bowtie nanoantenna (Au) with and without the MIM configuration.

it is important to predict the resonance wavelength shifts because of the insulator layer effect. To study the blue-shift effect of the resonance wavelength, because of the sapphire spacer thickness, we perform another simulation. A bowtie nanoantenna with the specifications in Fig. 1(b) and a fixed 20-nm Au metal film with an insulator thickness of 10, 30, and 70 nm are considered. Moreover, the simulation results for a bowtie nanoantenna in vacuum is presented (no MIM). FE factors in the wavelength range of 600–1200 nm for above-insulator layers are evaluated and the results are shown in Fig. 4. The increase in the spacer thickness decreases the near-field coupling strength in the spacer, causing blue shift in the resonance wavelength. The resonance peak position of the MIM structure with a 70-nm sapphire spacer is at 800 nm, whereas the peak position in the 30-nm layer is located at 900 nm. The simulation results are in good agreement with the results in Ref. [25].

Due to the near-field interaction between bowtie nanoantennas and their images in the gold layer, it is important to

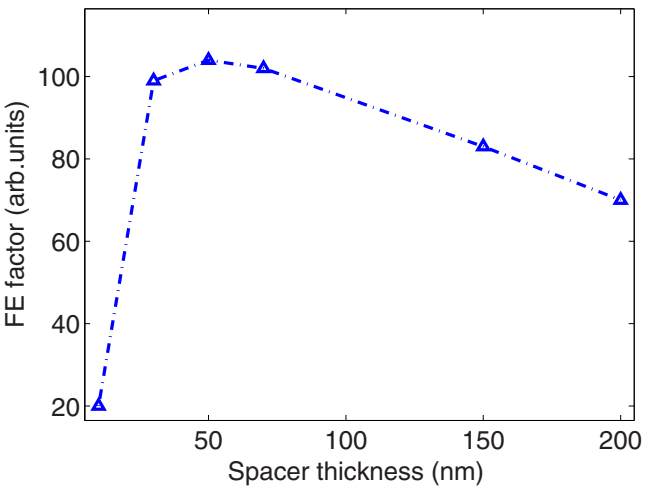

FIG. 5. Field enhancement factor vs spacer thickness for single Au bowtie nanoantennas in the MIM structure.

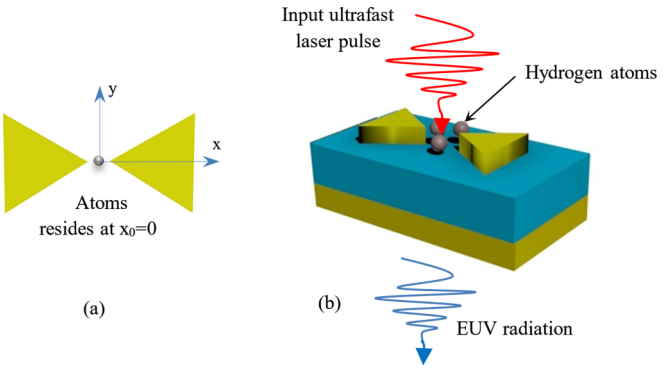

FIG. 6. (a) Position of atoms in the gap. (b) Sketch of the HHG device.

investigate the role of the sapphire spacer thickness on FE factors for a MIM structure. We considered the structure in Fig. 1(b) with a fixed 20-nm Au layer and sapphire spacers of different thicknesses, i.e., 10, 30, 50, 70, 150, and 200 nm. As illustrated in Fig. 5, the optimum spacer layer thickness for the MIM structure is 50 nm for a single bowtie nanoantenna and the related FE factor is 120. Due to the decreased scattering and absorption efficiencies for spacer layers of more than 70 nm (for example, 200 nm), the FE factors will be decreased. Comparing the peak values of FE factors in Figs. 2(a) and 5, one can conclude that the presence of a Au layer will increase the FE factor from 72 to 108.

V. HIGH-ORDER-HARMONIC GENERATION

In this section, the HHG spectrum of a hydrogen atom near metal nanostructures is described. To verify our scheme, we investigate HHG by numerically solving the 1D TDSE using the Crank-Nicolson method [34]. For horizontal polarized fields, the case under study here, the dynamics of an atomic electron is mainly along the direction of the laser electric field, and as a result, it is a good approximation to employ the Schrödinger equation in one spatial dimension.

In the 1D TDSE model, quantum diffusion is neglected, and also the efficiency of the harmonic will be altered, while the harmonic cutoff will be unchanged. The quantum diffusion is related to the spatial extension (spreading) of electron, i.e., the wave-packet dependency on the angular momentum channel l and the Laplace operator effect on the electron wave packet. By ignoring quantum diffusion, the ionization and recombination of the electron wave packet will be changed. Rae *et al.* investigated HHG spectra using two models. The first is in one dimension with an approximate hydrogenic soft-core potential and the second is in three dimensions with a Coulomb potential. As a result, the intensity of the highest-order harmonic in one dimension is about two orders higher in comparison with that in 3D models [35]. Although the ionization rates in the two models differ, the harmonic spectra and the positions of the cutoff are remarkably similar. Only a relatively small number of angular momentum states is needed in the 3D calculation to give a reliable estimate of the cutoff, even for intensities at which there is strong ionization. It is worth stressing, however, that despite the large difference in final ionization between the 1D and the 3D models, the harmonic spectra appear very similar. The position of the cutoff depends primarily on the intensity, and not on the rate of ionization. The related interaction Hamiltonian term is $V_I(x,t) = xE(x,t)$, where $E(x,t) = E(t)g(x)$ and $g(x)$ represents the functional form of the inhomogeneous electric field, which can be obtained by fitting the actual electric field [14]. First, we use the extracted data from the simulations and draw the 1D enhanced field distribution on the x axis (in the center of the gap between the edges of the elements) to estimate the nonlinear fitted $g(x)$ distribution of the enhancement factor. The initial position of hydrogen atoms and a schematic of the interaction of the laser field and hydrogen atoms near our nanostructure are shown in Figs. 6(a) and 6(b), respectively. We assume that the single target atom is initially in the x_0 position. Here we consider $x_0 = 0$, which corresponds to the center of the gap. In Sec. V A, the effect of atom positions on the HHG spectrum is investigated.

In our first set of simulations, the HHG spectrum of a single bowtie nanoantenna in three arrangements—in vacuum, on sapphire, and in a MIM structure (as mentioned in Secs. IV A and IV B)—is investigated. To do this, the best results for a nanobowtie on sapphire [from Fig. 2(a); 70-nm sapphire] and in a MIM structure (from Fig. 5; 50-nm sapphire) are selected. The electric field distributions in the nanobowtie gap, $g(x)$ (a 10-nm gap is fixed for all simulations), for three arrangements are shown in Fig. 7(a). In this figure, the dashed

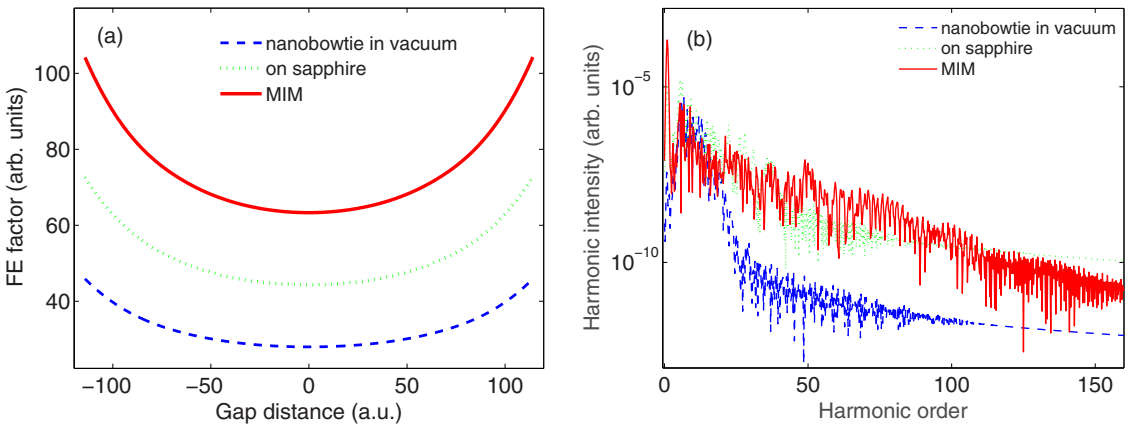

FIG. 7. (a) Electric field distribution in the nanobowtie gap for three arrangements. (b) The related HHG spectra.

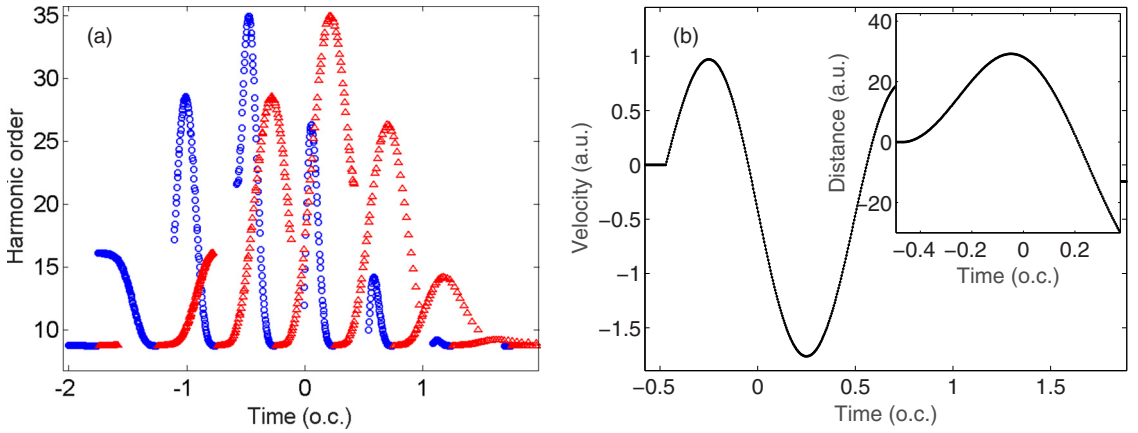

FIG. 8. (a) Total energy of the electron (expressed in harmonic order) driven by the enhanced field and plotted as a function of the ionization time (blue circles) or the recollision time (red triangles). (b) Evolution of the electronic wave-packet velocities and trajectories (inset).

blue curve shows the field distribution in the gap of the bowtie nanoantenna in vaccum and the maximum FE factor is about 45. The dotted green curve represents the field distribution in the gap of the bowtie nanoantenna installed on a 70-nm sapphire layer and shows an FE factor of about 70. Finally, the red curve is related to the MIM structure with a 50-nm sapphire layer and the corresponding FE factor is 108. The corresponding HHG spectrum of the above three structures is shown in Fig. 7(b). The maximum cutoff frequency is about 20 for the bowtie nanoantenna in vacuum (blue curve), about 45 for the bowtie nanoantenna on a sapphire layer (green curve), and about 150 for a MIM structure (red curve). As shown in Fig. 7(b) the HHG cutoff frequency is extended more than twice, with respect to the vacuum, and more than 3.33 times with respect to the nanobowtie installed on sapphire, which can be related to the coupled plasmon-polariton effect of the MIM structure.

Next, we continue our work with a semiclassical three-step model simulation to investigate the underlying mechanism of the extension of the HHG plateau [36] in Fig. 7(b). In Fig. 8(a), for a nanobowtie on sapphire, and Fig. 9(a) for a nanobowtie on MIM illuminated by a laser pulse, the dependence of the harmonic order on the ionization (blue circles) and emission times (red triangles) are plotted. The maximum energy of the photoelectrons is emitted only near the peaks marked with the maximum harmonic orders of 25 and 250, respectively. These results agree with the 1D TDSE predictions [see Fig. 7(b)]. Furthermore, Figs. 8(b) and 9(b) show the dynamics of trajectories and velocities of the electron propagating in laser fields which emit the maximum photon energy.

Based on the results in Fig. 7(b) for sapphire and MIM structures, the strongest photons (harmonic cutoff) are emitted from electrons that were born at −0.47 and −0.58 optical cycle (o.c.) [Figs. 8(a) and 9(a)], then the electrons are kept away from the parent ion and stop at times of −0.04 and −0.05 o.c., corresponding to 29.2- and 93.9-a.u. distances [Figs. 8(b) and 9(b)], and, finally, recombined with the parent ion at 0.22 and 0.24 o.c. The collision velocities of the electrons [Figs. 8(b) and 9(b)] are −1.7 and −4.28 a.u., which lead to the emission of harmonic cutoffs 35 and 170, correspondingly. This high velocity of electrons in MIM structures (in comparison with sapphire) is due to the high electric field amplitudes sensed by the electrons in the return path. According to Figs. 8(a) and 9(a), the electric fields sensed by the returning electrons from start to recombination for sapphire and MIM, respectively, are 0.0181 to 0.0125 and 0.1355 to 0.0050 a.u. Also, the elapsed times for the return trajectories are 0.046 and 0.296 o.c.

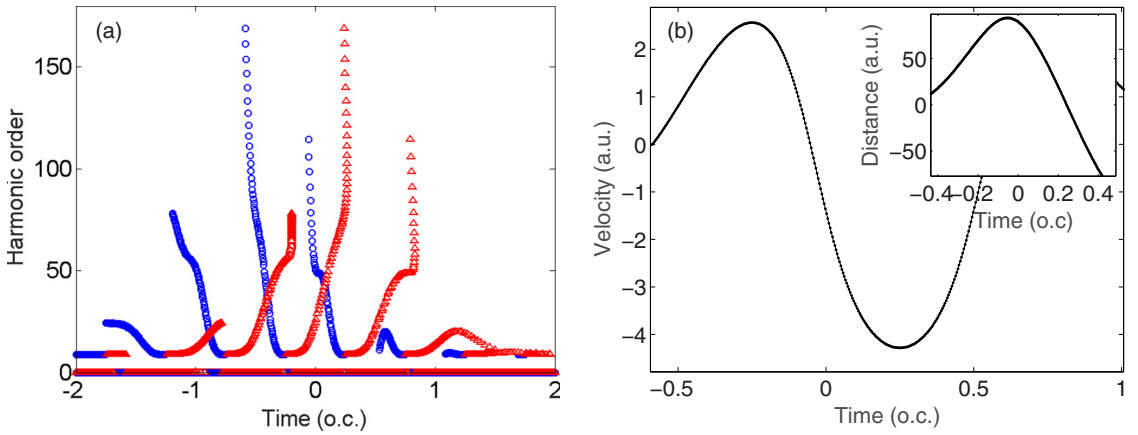

FIG. 9. Same as Fig 8, but here the nanobowtie is in a MIM structure.

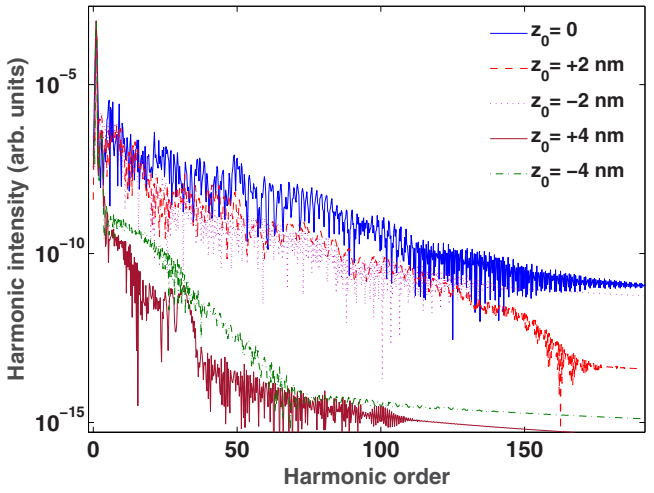

FIG. 10. Effect of atom positions in the gap region on the HHG spectrum.

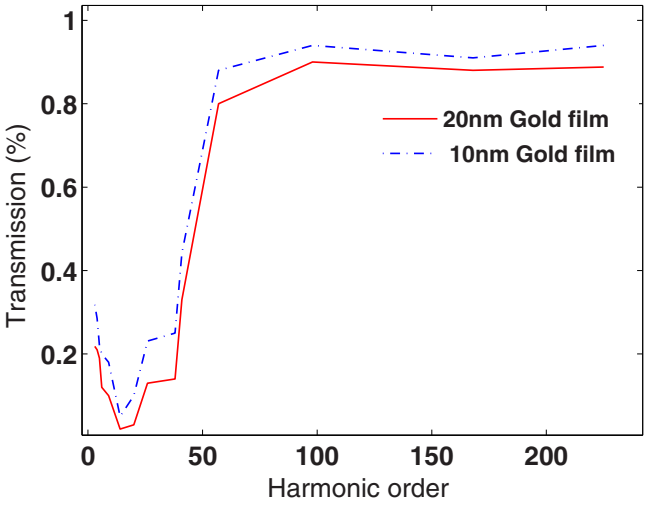

FIG. 11. Transmission properties of Au film vs harmonic orders for various Au thicknesses.

Therefore, the electric field sensed by the returned electrons and, also, the return time for the MIM structure have a maximum value in comparison with the sapphire values. As a result, the MIM structure considerably increases the collision kinetic energy and, hence, the emitted photon energy.

A. The effect of atom position on the HHG spectrum

In the previous section, we performed the calculations for harmonic emission inside the nanogap, taking hydrogen atoms as the target. It was assumed that the single target atom was initially in the z_0 position. Here we consider that the gap between the apexes of the bowtie nanoantenna is 10 nm. Therefore, $z_0 = 0$ corresponds to the center of the nanogap. In this section, we investigate the HHG spectrum in five positions: $z_0 =$ 0, ± 2, ± 4 nm. Figure 10 monitors the harmonic spectrum attainable from hydrogen atoms placed in five positions inside the nanostructure gap. It is clear that both the overall yield and the cutoff frequencies become different when we move from the center to the metal surface. This difference can be related to the different trajectories of electrons which move inside the inhomogeneous enhanced fields and various sensed fields. For a more detailed explanation one can refer to Ref. [12].

B. Transmission and reflection properties of gold thin film

The optical properties of substrate materials is a critical parameter that determines the transmission and reflection values. Sapphire is an insulator material which is frequently used as a substrate to install metal nanoparticles in plasmonic assisted HHG devices with excellent transmission properties for different harmonic orders [2,37]. Hence in this work we used sapphire as insulator in the MIM structure. Because of the good transmission properties of this material in the EUV spectrum, it is frequently used in practical HHG devices so we do not investigate its transmission properties and just consider the gold film reflection and transmission properties. Optical constants in a wide range of frequencies, from EUV to visible, are available in the literature. In this work we use the optical constants of gold film presented by Hagemann *et al.* and the transmission and absorption properties of our scheme are calculated [38]. We assume that the incident angle of the driving ultrafast laser pulse is normal to the metal surface and the HHG radiation also is propagated in the same direction. The transmission of 10- and 20-nm gold films is shown in Fig. 11. It is clear that reducing the thickness of the gold film will increase its transmission. Moreover, because of the selective properties of gold film in low transmission, below orders of 50, it can be used as a device to select higher HHG orders and block lower orders.

VI. CONCLUSION

In this paper we have attempted to extend the HHG spectrum of atomic hydrogen gas using surface plasmon polaritons. We have utilized the coupling between SPPs and LSPPs in a special type of nanostructure to extend the high harmonic orders. The proposed plasmonic device is made of a bowtie nanoantenna installed on two layers: the upper layer is sapphire and the underlayer is a 20-nm Au metal film that supports the plasmon-polariton modes. We have analyzed the effect of surface plasmon-polariton coupling in different nanostructures and their effect on electric field enhancement factors in the gap of bowtie nanoantennas. The resultant field enhancement factors enable us to extend the harmonic cutoffs. We found that the maximum harmonic order for an isolated nanobowtie on an MIM structure is about 170, which is a good modification of the HHG process by low-intensity ultrashort laser pulses. It is possible to arrange MIM structures in a 2D array and use it as an efficient target for the HHG process.

[1] A. Husakou, S. J. Im, and J. Herrmann, Phys. Rev. A **83**, 043839 (2011).

[2] S. Kim, J. Jin, Y. J. Kim, I. Y. Park, Y. Kim, and S. W. Kim, Nature Lett. **453**, 757 (2008).

[3] M. Mohebbi, Phys. Rev. A **91**, 023835 (2015).
[4] M. Mohebbi, Appl. Phys. B **122**, 39 (2016).
[5] H. Fischer and O. J. F. Martin, Opt. Express **16**, 9144 (2008).
[6] N. Hooshmand, M. A. El-Sayed, and J. A. Bordley, Nano Lett. **15**, 3391 (2015).
[7] E. Hao and G. C. Schatz, J. Chem. Phys. **120**, 357 (2004).
[8] F. Lee, D. W. Brand, Y. A. Urzhumov, H. Wang, J. Kundu, N. J. Halas, J. Aizpurua, and P. Nordlander, ACS Nano **2**707 (2008).
[9] I. Y. Park, S. Kim, J. Choi, D. H. Lee, Y. J. Kim, M. F. Kling, M. I. Stockman, and S. W. Kim, Nat. Photon. **5**, 677 (2011).
[10] M. F. Ciappina, S. S. Aćimović, T. Shaaran, J. Biegert, R. Quidant, and M. Lewenstein, Opt. Express **20**, 26261 (2012).
[11] T. Shaaran, M. F. Ciappina, R. Guichard, J. A. Pérez-Hernández, L. Roso, M. Arnold, T. Siegel, A. Zaïr, and M. Lewenstein, Phys. Rev. A **87**, 041402(R) (2013).
[12] I. Yavuz, Phys. Rev. A **87**, 053815 (2013).
[13] S. H. Hekmatara, M. Mohebbi, and J. Rahpeyma, RSC Adv. **4**, 59064 (2014).
[14] H. Ebadian and M. Mohebbi, Appl. Opt. **55**, 8035 (2016).
[15] F. Ye, J. M. Merlo, J. M. Burns, and M. J. Naughton, Nanophotonics **3**, 33 (2014).
[16] Y. Chu, M. G. Banaee, and K. B. Crozier, ACS Nano **4**, 2804 (2010).
[17] J. Cesario, R. Quidant, G. Badenes, and S. Enoch, Opt. Lett. **30**, 3404 (2005).
[18] H. T. Miyazaki and Y. Kurokawa, Phys. Rev. Lett. **96**, 097401 (2006).
[19] T. J. Seok, A. Jamshidi, M. Kim, S. Dhuey, A. Lakhani, H. Choo, P. J. Schuck, S. Cabrini, A. M. Schwartzberg, J. Bokor, E. Yablonovitch, and M. C. Wu, Nano. Lett. **11**, 2606 (2011).
[20] D. K. Gramotnev, A. Pors, M. Willatzen, and S. I. Bozhevolnyi, Phys. Rev. B **85**, 045434 (2012).
[21] Y. Chu, E. Schonbrun, T. Yang, and K. B. Crozier, Appl. Phys. Lett. **93**, 181108 (2008).
[22] Y. Chu and K. B. Crozier, Opt. Lett. **34**, 244 (2009).
[23] N. A. Hatab, C. H. Hsueh, A. L. Gaddis, S. T. Retterer, J. H. Li, G. Eres, Z. Zhang, and B. Gu, Nano Lett. **10**, 4952 (2010).
[24] F. Zhou, Y. Liu, and W. Cai, Opt. Lett. **39**, 1302 (2014).
[25] L. Lin and Y. Zheng, Sci. Rep. **5**, 14788 (2015).
[26] A. Sundaramurthy, K. B. Crozier, G. S. Kino, D. P. Fromm, P. J. Schuck, and W. E. Moerner, Phys. Rev. B **72**, 165409 (2005).
[27] S. Dodson, M. Haggui, R. Bachelot, J. Plain, S. Li, and Q. Xiong, J. Phys. Chem. Lett. **4**, 496 (2013).
[28] B. Grzeskiewicz, K. Ptaszynski, and M. Kotkowiak, Plasmonics **9**, 607 (2014).
[29] T. Mori, K. Yamaguchi, Y. Tanaka, Y. Suzaki, and M. Haraguch, Opt. Rev. **23**, 260 (2016).
[30] K. Yamagucci, T. Inoue, M. Fuji, M. Haragucci, T. Okomoto, M. Fukui, S. Seki, and S. Sagava, Chinese Phys. Lett. **24**, 2934 (2007).
[31] A. Taflove and S. C. Hangess, *Computational Electrodynamics: The Finite-Difference Time-Domain Method* (Artech House, London, 2000).
[32] D. M. Sullivan, *Electromagnetic Simulation Using the FDTD Method* (Wiley, New York, 2013).
[33] H. C. Kim and X. Cheng, Opt. Express. **17**, 17234 (2009).
[34] W. Y. Hong, P. X. Lu, and W. Cao, J. Phys. B **40**, 2321 (2007).
[35] S. C. Rae, X. Chen, and K. Burnett, Phys. Rev. A **50**, 1946 (1994).
[36] P. B. Corkum, Phys. Rev. Lett. **71**, 1994 (1993).
[37] S. Han, H. Kim, Y. W. Kim, Y. J. Kim, S. Kim, I. Y. Park, and S. W. Kim, Nat. Commun. **7**, 13105 (2016).
[38] H. J. Hagemann, W. Gudat, and C. Kunz, J. Opt. Soc. Am. **65**, 742 (1975).